Final Draft

of the original manuscript

Aliyev, E.; Warfsmann, J.; Tokay, B.; Shishatskiy, S.; Lee, Y.; Lillepaerg, J.; Champness, N.; Filiz, V.:

Gas Transport Properties of the Metal–Organic Framework (MOF)-Assisted Polymer of Intrinsic Microporosity (PIM-1) Thin-Film Composite Membranes.

In: ACS Sustainable Chemistry & Engineering. Vol. 9 (2021) 2, 684 - 694.

First published online by ACS: 22.12.2020

https://dx.doi.org/10.1021/acssuschemeng.0c06297

Gas transport properties of the Metal-Organic Framework (MOF) assisted Polymer of Intrinsic Microporosity (PIM-1) thin-film composite membranes

Elvin Aliyev[†], Jan Warfsmann[‡], Begum Tokay[‡], Sergey Shishatskiy[†], Young-Joo Lee[§], Jelena Lillepaerg[†], Neil R. Champness[ǀ], Volkan Filiz[,†]*

[†] Institute of Polymer Research, Helmholtz-Zentrum Geesthacht, Max-Planck-Str. 1, 21502 Geesthacht, Germany

[‡] Department of Chemical and Environmental Engineering, Faculty of Engineering, University of Nottingham, University Park, NG7 2RD, Nottingham, UK

[§] Institute of Inorganic and Applied Chemistry, Department of Chemistry, University of Hamburg, Martin-Luther-King-Platz-6, 20146 Hamburg, Germany

[ǀ] School of Chemistry, University of Nottingham, University Park, NG7 2RD, Nottingham, UK

AUTHOR INFORMATION

Corresponding Author

*E-mail address: volkan.filiz@hzg.de (Volkan Filiz)

ABSTRACT

The current study summarizes the findings of the single gas transport performances of the mixed matrix thin-film composite membranes (TFCM) consisting of metal-organic frameworks (MOFs) incorporated into the polymer of intrinsic microporosity (PIM-1). The Mg-MOF-74, MIL-53, TIFSIX-3, and $Zn_2(bim)_4$ were investigated as stand-alone materials and as incorporated into the PIM-1 polymer matrix serving as a selective layer of thin-film composite membranes by various methods: Fourier-transform infrared spectroscopy (FTIR), solid-state NMR (SSNMR), X-ray diffraction (XRD), thermogravimetric analysis (TGA), and scanning electron microscopy (SEM). The effect of MOF-loading and nature on mixed-matrix membrane (MMM) morphology and operation were analyzed by varying the MOF content in the polymer matrix from 2 to 10 wt.% with respect to dry polymer weight. The results show that the incorporation of MOFs into the PIM-1 polymer matrix boosts the permeance and selectivity of H_2 and O_2 over N_2, and the prepared PIM-1/TIFSIX_4 mixed matrix membrane shows better separation performance for CO_2/CH_4 than that of pure PIM-1. Such membranes can be good candidates for ammonia purge gas, oxygen enrichment, and acid gas treatment applications.

KEYWORDS: mixed matrix membrane, metal-organic framework, polymers of intrinsic microporosity, gas separation, thin-film composite membrane, gas adsorption

SYNOPSIS

The thin-film composite membranes based on PIM-MOF potentially allow for improved and sustainable gas separation combined with low energy consumption.

INTRODUCTION

Gas separation with polymer-based membranes is a promising approach due to its low relative energy consumption, ease of operation, and cost-effectiveness. The main challenge in the operation of the pristine solution-diffusion based membranes, based on, *e.g.*, the polymer of intrinsic microporosity (PIM), is the lack of selectivity and permeability, which is usually below the Robeson upper bound [1]. Such a phenomenon has motivated the development of new gas separation membranes known as mixed-matrix membranes (MMM) [2-3] synergistically comprising advantages of highly selective but mechanically disadvantaged porous organic or inorganic materials, and mechanically stable but having limited selectivity polymers. The nanoporous fillers such as "drilled" graphene, "defective" graphene oxide [4], and their modifications [5-7], metal-organic frameworks, etc. being embedded into the polymer matrix positively influence the gas transport properties of the polymer membranes.

PIM-1 possesses high free volume build of large, well interconnected free volume elements that are formed as a result of the highly contorted and extremely rigid polymer backbone structure [8]. The presence of the large free volume elements makes this polymer more attractive in terms of highly permeable polymer membrane preparation. The large free volume providing relatively low selectivity can be utilized for the delivery of penetrants to the nanoporous filler particles in order to improve the transport properties of the PIM-1 membranes [9-10].

Recently, metal-organic frameworks (MOFs) have received a growing interest as a potential filler in the field of MMMs. This new group of materials made by the covalently linking of the

metal centers to organic building blocks [11]. The metal centers form the vertices of a framework, while organic linkers generate a porous structure with the defined structure and shape, which plays an important role in mass transport.

Due to the presence of nanometer-scale pores, MOFs are used in different applications such as water purification and gas separation by adsorption. Akpinar *et al.* [12] used three different MOFs for water purification from atrazine contamination. Experiments conducted on MOF supported polymers showed that the utilization of a continuous MOF layer exhibits much higher technical barrier than polymer gutter layer in 30 nm-thick polymer membranes with an ideal selectivity of 34 for CO_2/N_2 gas pair [13]. ZIF-8 membranes formed inside porous γ - Al_2O_3 support showed a marked hydrogen separation performance with a maximum H_2/CO_2 separation factor of ~9.9 at 250 °C [14]. The exfoliated two-dimensional $Zn_2(bim)_4$ showed an H_2/CO_2 selectivity greater than 200 [15]. Recently synthesized UTSA-220 MOF nanoparticles exhibit high C_2H_2 uptake capacity, which is very interesting in terms of acetylene separation from light hydrocarbons in downstream industrial applications [16]. Go *et al.* [17] revealed that in-situ grown ZIF-7 membranes show higher selectivity (~16) for H_2/CO_2 than ZIF-7 membranes prepared by other methods.

MOFs present good compatibility with the polymer due to its organic nature with a low density [18], which makes them a potential filler for the gas separation purposes. The organic nature of the MOF allows one to introduce various functional groups having an affinity to *e.g.,* CO_2. Tien-Binh [19] *et al.* showed that Mg-MOF-74 crosslinked PIM-1 shows better gas transport properties, compared to PIM-1 due to the 1-D hexagonal nanochannels with a 1.1 nm diameter influence strongly the CO_2 permeability and selectivity. Amine modified ZIF-8 and polyamide thin-film nanocomposite membranes prepared by in-situ interfacial polymerization show high separation performance for gas pairs, as reported by Yu [20]. ZIF-11 incorporated 6FDA-DAM mixed matrix

membranes exhibited high permeability for H_2, CO_2, and CH_4 gases [21]. Experiments conducted on ZIF-71 nanoparticle incorporated 6FDA-Durene yielded an increase in the CO_2 permeability by three times [22]. Two-dimensional, layered CuBDC nanosheets incorporated ultrathin PIM-1 mixed matrix membrane exhibited a CO_2/CH_4 selectivity of 15.6, and CO_2 permeance surpassed the pure PIM-1 performance [23]. Mixed-matrix membranes based on UiO-66 loaded PIM-1 shows high selectivity for CO_2/CH_4 gas pairs surpassing the Robeson upper bound [24]. ZIF-8 incorporated microporous polyimide polymer with a Tröger's Base presents enhanced separation for H_2/N_2 and H_2/CH_4, surpassing the state-of-the-art 2008 Robeson upper bound [25]. The MMMs prepared with the incorporation of the ultrathin α-$Ni(im)_2$ nanosheets into the PEBAX MH 1657 polymer matrix performed an enhanced CO_2/CH_4 selectivity based on molecular sieving properties. Thus, the addition of 2 wt.% α-$Ni(im)_2$ nanosheets increases the selectivity of CO_2 over CH_4 with a separation factor of 33.4 without compromising the CO_2 permeability [26]. A mixed-matrix membrane composed of ZIF-94 filler and 6FDA-DAM polymer matrix presented the increasing trend in CO_2 permeability, depending on filler loading. It was revealed that at 40 wt.% loading, the CO_2 permeability reached at 2310 Barrer and the CO_2/N_2 mixed gas selectivity was ~22 [27].

The current paper investigates the single gas transport properties of MMMs, containing Mg-MOF-74, MIL-53, TIFSIX-3, and layered $Zn_2(bim)_4$ particles embedded into the PIM-1 polymer matrix. The selected MOF structures have range of pore sizes (0.2-1.1 nm) and affinity towards CO_2 that influences the permeability and selectivity of the membrane separation properties. For the rationalization of the incorporation of these metal-organic frameworks into the PIM-1 polymer matrix, these questions were taken into consideration:

a) How would the dimensionality of the particles influence the gas transport properties of the mixed matrix membranes?

b) How do the pore sizes affect the gas transport through such kind of membranes?

c) Can we develop highly permeable and selective membranes for the sustainable progress in the industry?

Our results revealed that the MOF inclusion improved both permeability and selectivity of composite membranes for selected gases. In addition, it was determined that the incorporation of layered $Zn_2(bim)_4$ particles into the PIM-1 polymer matrix substantially decreases the aging phenomena of the PIM-1, which is a drawback for these membranes. Thus, PIM-1 is considered as a highly permeable and selective material for gas separation technology. Such kind of an improvement regarding the decrease in the aging of the membrane opens up a new way for the sustainable development of the industry.

EXPERIMENTAL SECTION

Materials. Magnesium acetate tetrahydrate ($Mg(CH_3COO)_2 \cdot 4H_2O$) (99%), 2,5-dihydroxyterephthalic acid (H_4DHTP) (98%), aluminum nitrate nonahydrate ($Al(NO_3)_3 \cdot 9H_2O$), 1,4-benzenedicarboxylic acid (H_2BDC) (>98%), nickel nitrate hexahydrate ($Ni(NO_3)_2 \cdot 6H_2O$), nickel(II) carbonate (basic) hydrate ($NiCO_3 \cdot 2Ni(OH_2) \cdot nH_2O$), pyrazine, Hexafluorotitanic acid (H_2TIF_6, 60 wt.% in water), and zinc nitrate hexahydrate ($Zn(NO_3)_2 \cdot 6H_2O$, 98%) were purchased from Sigma Aldrich. Benzimidazole (BI, 99%) was purchased from Alfa Aesar. The solvents *N,N*-Dimethylformamide (DMF), and methanol (MeOH) were purchased from Fischer Scientific. All chemicals were reagent grade and used as received. Deionized water (DI water) was collected from Millipore Direct-Q 5 UV water purification system.

Synthesis of Mg-MOF-74 powders. An elevated temperature method was applied for the synthesis of Mg-MOF-74 crystals reported by Campbell *et al*. [28]. This technique resulted in the reduction of the synthesis time. In a typical synthesis, 0.39 to 0.41 g H_4DHTP was completely

dissolved in 10 mL DMF using a magnetic stirrer. Metal salt solutions were prepared by complete dissolution of between 1.15 to 1.21 g magnesium acetate tetrahydrate in a 10:0:0 mL of the mixture of DMF:water:ethanol.

Synthesis of MIL-53 powders. MIL-53 was synthesized according to a synthesis protocol described earlier [29]. In a brief description, $Al(NO_3)_3 \cdot 9\ H_2O$ (5.99 mmol; 2.246 g) and H_2BDC (5.38 mmol; 0.895 g) were mixed together and dispersed in 30 mL of solvent (DMF and MeOH) and stirred vigorously at room temperature for 15 min and transferred to a 45 mL Parr Teflon® lined stainless steel reaction vessel. The reaction mixture was heated to 150 °C for 5 h, and the obtained product was separated by centrifugation (4500 rpm for 30 min). The solution was decanted, and the powder was washed with DMF (2 x 50 mL) and acetone (1 x 50 mL). The powder was dried at 150 °C for 17 h. The removal of the unreacted starting materials and residue solvent were performed by the heating of the powder at 333 °C for 3 days.

Synthesis of TIFSIX-3. The synthesis of TIFSIX-3 was performed via two-step procedure. In the first step, $NiCO_3 \cdot 2Ni(OH_2) \cdot 4H_2O$ (3 g, 4.93 mmol) was dissolved in 15 mL water containing flask for 15 min at room temperature (RT). Subsequently, 60% aqueous solution of H_2TiF_6 (1.5 g, 10.98 mmol) was added into the flask, followed by 5 minutes stirring, and the resulting final mixture was stored at RT for 2 days. A green and highly hygroscopic solid was obtained by the evaporation of the solvent at 90 °C for 24 h after filtration of the mixture.. The resulted powder kept at 90 °C until a solid green product was formed. After approx. 72 h, 2.152 g (87% yield) powder ($NiTiF_6$) was collected. The next synthesis procedure was done by the method presented previously elsewhere [30]. Briefly, $NiTiF_6$ (0.5 g; 2.22 mmol) and pyrazine (1 g; 12.48 mmol for excess pyrazine or 0.356 g; 4.44 mmol for equimolar reaction) were dissolved in 5 mL of solvent (water, MeOH, acetone or DMF) each and stirred at RT. After 15 min, these two solutions were

mixed together and stirred for an additional 15 min. The reaction mixture was poured into a beaker and covered with a lid (for RT reaction) or poured into a 45 mL Teflon®-lined stainless steel pressure vessel (Parr Instruments 4744 General Purpose Acid Digestion Vessel, for 85 °C reaction). Centrifugation at 4000 rpm for 30 min was utilized for the separation of the product, after 24 h reaction (in DMF at 85 °C for 15 h), and the solution was decanted. The product was washed with water and activated in MeOH for 3 days. The product was obtained as a purple powder after heating in the vacuum at 120 °C for 24 h.

Synthesis of $Zn_2(bim)_4$ particles. $Zn_2(bim)_4$ nanosheets were synthesized via a hydrothermal method [15]. Thus, 0.3 g (1.00 mmol) of $Zn(NO_3)_2$ 6 H_2O was mixed with 0.77 g (6.52 mmol) of benzimidazole in a 250 mL round-bottom flask and dissolved in 100 mL anhydrous DMF. After dissolution, the flask stirred for 48 hours at room temperature, and it was subsequently kept still for another 2 days. The product was centrifuged at 10000 rpm for 30 minutes in order to separate the synthesized ZIF-7 nanocrystals from DMF. The ZIF-7 nanocrystals washed carefully with ultrapure water and methanol. The yield was 55% with respect to Zn^{2+} salt. After drying, 0.15 grams of ZIF-7 nanocrystals placed in a 100 mL round-bottom flask and refluxed for 24 hours at 100 °C in water. The product was vacuum-filtered on Qualitative Grade 1 Whatman filter paper, washed with ultrapure water, methanol, and dried. The product is denoted as $Zn_2(bim)_4$, and the yield was 75% with respect to ZIF-7 nanocrystals.

Thin-film composite membrane preparation. The thin-film composite membranes (TFCM) from PIM and MOF particles were cast on microporous ultrafiltration polyacrylonitrile (PAN) support (made in-house, an average pore size of 22 nm and 15% surface porosity, polyester non-woven as mechanical stability provider) using a house-built membrane casting apparatus [31]. The particles of Mg-MOF-74, MIL-53, TIFSIX-3, and $Zn_2(bim)_4$ were dispersed in 1wt.% PIM-1

solution in THF at 2, 4, 6, 8 and 10 wt.% loadings with respect to polymer dry weight. After the preparation of the composite dispersions, they were sonicated for 30 minutes in the sonication bath before casting. The selective layer deposition was done by a modified dip-coating method. Thus, the porous support was first brought into contact with the polymer solution and then lifted by 1-2 mm. This caused to the formation of a meniscus between the porous membrane and solution surface. The selective layer was formed at ambient conditions by dragging the polymer solution (at 1.56 m/min speed) out of the meniscus. As a result, the uniform, and reproducible coating was achieved. The evaporation of the solvent was not controlled or influenced as the formed membrane was allowed to dry at ambient conditions.

RESULTS AND DISCUSSION

Characteristics of the MOF fillers. The FTIR experiments (Figure S1) were conducted for the synthesized ZIF-7 and $Zn_2(bim)_4$ particles to understand the coordination of benzimidazole molecules to Zn^{2+} metal centers. IR analysis of the benzimidazole molecules conducted by Pashchevskaya *et al.* [32] showed that in-plane and out-of-plane N-H stretching vibrations of the linker (benzimidazole molecule) are between 2540 and 3060 cm^{-1}. However, such stretching vibrations overlap with the combination bands of C=C stretching and C-H in-plane bending vibrations of the benzimidazole molecule, making separation of these vibrations complicated. The presence of the combination bands was firstly described by Mohan *et al.* [33]. They have indicated that the benzimidazole [33] shows the stretching vibrations between 2900 and 3100 cm^{-1}, which are the combination bands of C=C stretching and C-H in-plane bending vibrations. Those peaks at 2900-3100 cm^{-1} are also seen for our materials. Since this stretching vibration range belongs to the aliphatic compounds and the synthesized compounds do not possess any aliphatic groups, they are

assumed as the combination bands of two different vibrations. For example, the peak at 2900 cm^{-1} is the combination band of the peaks at 1621 and 1273 cm^{-1}, which are C=C stretching and C-H in-plane bending vibrations of the benzene rings. The peak at 1772 cm^{-1} is not a stretching vibration of the carboxylic groups; thus, it can be attributed to the combination band of the N-H in-plane bending vibrations at 1545 cm^{-1} and out-of-plane (C-C-C) bending of the organic linker at 228 cm^{-1} [33]. Hence, the identification of the C-N and C=N stretching vibrations is a difficult task for the benzimidazole molecules. Mohan and Sundaraganesan [33] suggested that the C=N stretching vibration is at 1689 cm^{-1}; however, we did not observe this peak in the FTIR spectra of our materials. Moreover, the peak at 1675 cm^{-1} likely belongs to the C=O stretching vibrations of the residual DMF molecules that are trapped in the pores of the ZIF-7 nanoparticles. After the transformation of the ZIF-7 nanoparticles into the $Zn_2(bim)_4$ particles, this peak reduces significantly, which we claim it is the effect of the solvent exchange. According to the FTIR experiment, the residual DMF content in the pores of the ZIF-7 nanoparticles is ~10%. The C=C stretching vibrations of the aromatic ring is observed between 1241 and 1611 cm^{-1}. The strong peak at 750 cm^{-1} is attributed to the C-H out-of-plane bending vibration of the organic linker. Fully deprotonation of benzimidazole linker can occur in an alkaline medium. However, during the synthesis procedure, no alkaline medium was used. In finalizing the FTIR experiments, we can claim that some percent of the benzimidazole linkers were not deprotonated. Additionally, it is not claimed that the reaction was unsuccessful; thus, FTIR peaks below 600 cm^{-1} manifest the Zn-N stretching vibrations. The change in the feature of the spectra of ZIF-7 and $Zn_2(bim)_4$ particles demonstrates the structural difference between the particles.

For detailed information, ^{13}C solid-state NMR experiments were conducted for the synthesized ZIF-7 and $Zn_2(bim)_4$ particles (Figure 1). ZIF-7 shows two resonances for each carbon

with significant line broadening, suggesting the presence of two crystallographically different types of linkers and additional disorder. This is consistent with the crystallographic structure of ZIF-7 containing two crystallographically inequivalent linkers [34-35]. The spectra clearly show the existence of the solvent molecules trapped in the pores of the ZIF-7 nanoparticles, which is in agreement with the FTIR results. By contrast, a single sharp resonance is seen for each carbon of the $Zn_2(bim)_4$ sample, indicating that one type of crystallographically different linker exists in the layered structure. In comparison with the benzimidazole monomer, the signal for C1 carbon shifts to a high frequency significantly. This phenomenon suggests that the Zn atoms are coordinated via bonding to the nitrogen atoms. ^{13}C NMR results demonstrate that ZIF-7 and $Zn_2(bim)_4$ possess different crystallographic structure and crystallinity.

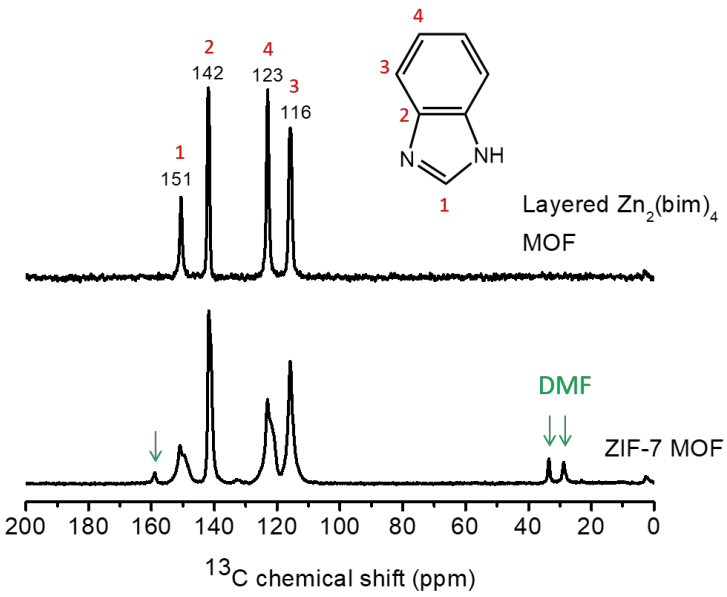

Figure 1. ^{13}C cross-polarization (CP) magic-angle spinning (MAS) NMR analysis of ZIF-7 and $Zn_2(bim)_4$ particles.

Thermogravimetric analysis showed that the ZIF-7 particles degrade in three steps while $Zn_2(bim)_4$ particles possess only one degradation step (Figure S2). The first degradation step for

ZIF-7 is observed between 30 and 200 °C, with a mass loss of ~8 %. This data overlaps with the FTIR and NMR data and confirms the existence of the trapped DMF molecules in the pores of the ZIF-7 particles. The second degradation step starts at 220 °C and ends at 700 °C with a ~37% mass loss, which corresponds to the decomposition of the framework. The last decomposition step could be attributed to the destruction of the benzimidazole molecules. Conversely, the $Zn_2(bim)_4$ particles are stable up to 550 °C. A plateau is followed by a ~46% mass loss between 550 and 800 °C, corresponding to the decomposition of the framework. The decomposition of TIFSIX-3 and Mg-MOF74 follows four degradation steps in comparison with the ZIF-7 and $Zn_2(bim)_4$ particles. The first degradation step with mass losses of ~10% for TIFSIX-3 and ~14% for Mg-MOF74 are recorded between 40 and 100 °C. This is related to water molecules adsorbed by the particles. The next degradation step is seen between 100 and 200 °C with a mass loss of ~10% in the case of TIFSIX-3, and between 100 and 350 °C with a mass loss of ~22% in the case of Mg-MOF74. Considering the boiling point of DMF (153 °C), it is highly accepted that in this temperature range the residual amount of the solvent evaporates from the particles. However, besides the solvent evaporation, the decomposition of the organic linker of Mg-MOF74 starts. The whole organic linker decomposition continues in the third step. The MIL-53 particles are stable up to 300 °C. It is followed with a ~32% mass loss corresponding the decomposition covalent bonds between the organic linkers and the metal centers of the framework in the temperature range between 300 and 500 °C. The next step (500-800 °C) with a ~46% mass loss is related to the decomposition of organic linkers.

Figure 2 depicts the X-ray powder diffraction spectra of the MOF particles both as experimental and simulated results. The spectra suggest that the transformation of the ZIF-7 particles into the $Zn_2(bim)_4$ particles leads to a strong crystal structure alteration. According to the

results it is suggested that the crystallinity of the particles is considerably different. Using the Scherrer equation, it was calculated that the crystal size of the ZIF-7 particles has significantly changed after transformation into the $Zn_2(bim)_4$ particles from 60 nm to 200 nm, respectively. The simulated XRD pattern also confirms the formation of an ordered structure.

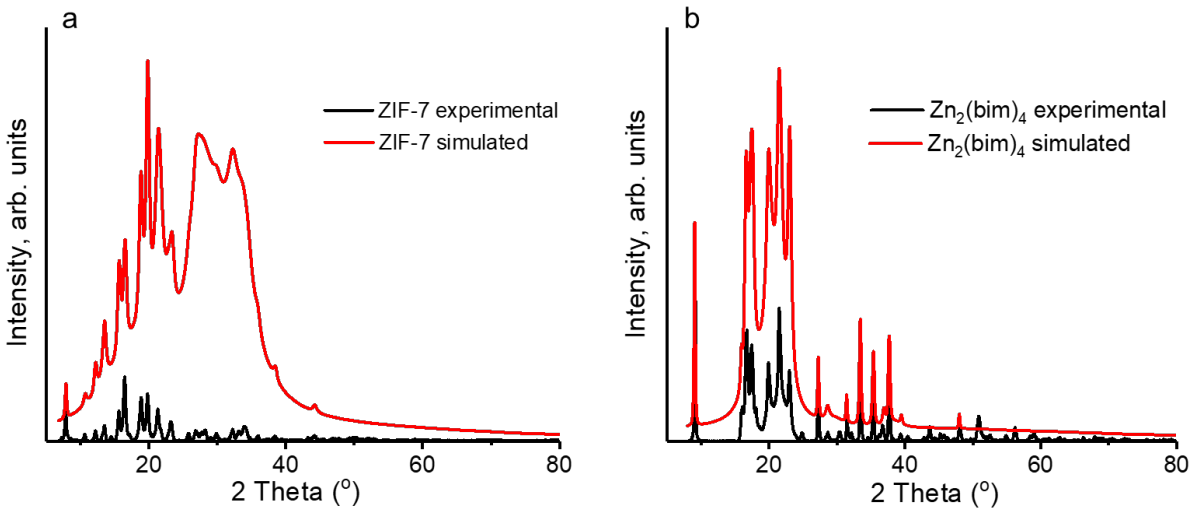

Figure 2. XRD pattern of the synthesized (a) ZIF-7 and (b) $Zn_2(bim)_4$ particles. Red curves show the PXRD simulated patterns.

A detailed explanation of XRD patterns of Mg-MOF-74, MIL-53, and TIFSIX-3 MOF particles is given elsewhere [28-30, 36-39]. The particle sizes of Mg-MOF-74, MIL-53, and TIFSIX-3 MOF particles used in this study were in consistent with the data reported previously.

SEM images and the EDX elemental mapping of the ZIF-7 and $Zn_2(bim)_4$ MOF particles are shown in Figure 3. The ZIF-7 particles have successfully transformed into $Zn_2(bim)_4$ particles, which possess the ordered structure with dimensions of approximately 1000×1000×200 nm. However, the EDX elemental mapping of the particles did not show much difference. Both samples showed that the amount of the elements distributed through the particles are the same and confirms the solely transformation of the crystalline shape. Peng *et al.* [15] revealed that such

particles have a layered structure. To support the argument we conducted exfoliation experiments and analyzed through the TEM microscopy (Figure S3). It was revealed that $Zn_2(bim)_4$ particles consist of layers and it is possible to exfoliate them. After exfoliation, a single layer is visible. SEM images of the Mg-MOF-74, MIL-53, and TIFSIX-3 MOF crystals are consistent with the previous reports. Crystals of such kinds of MOF particles possess spherical shapes and range in several micrometers.

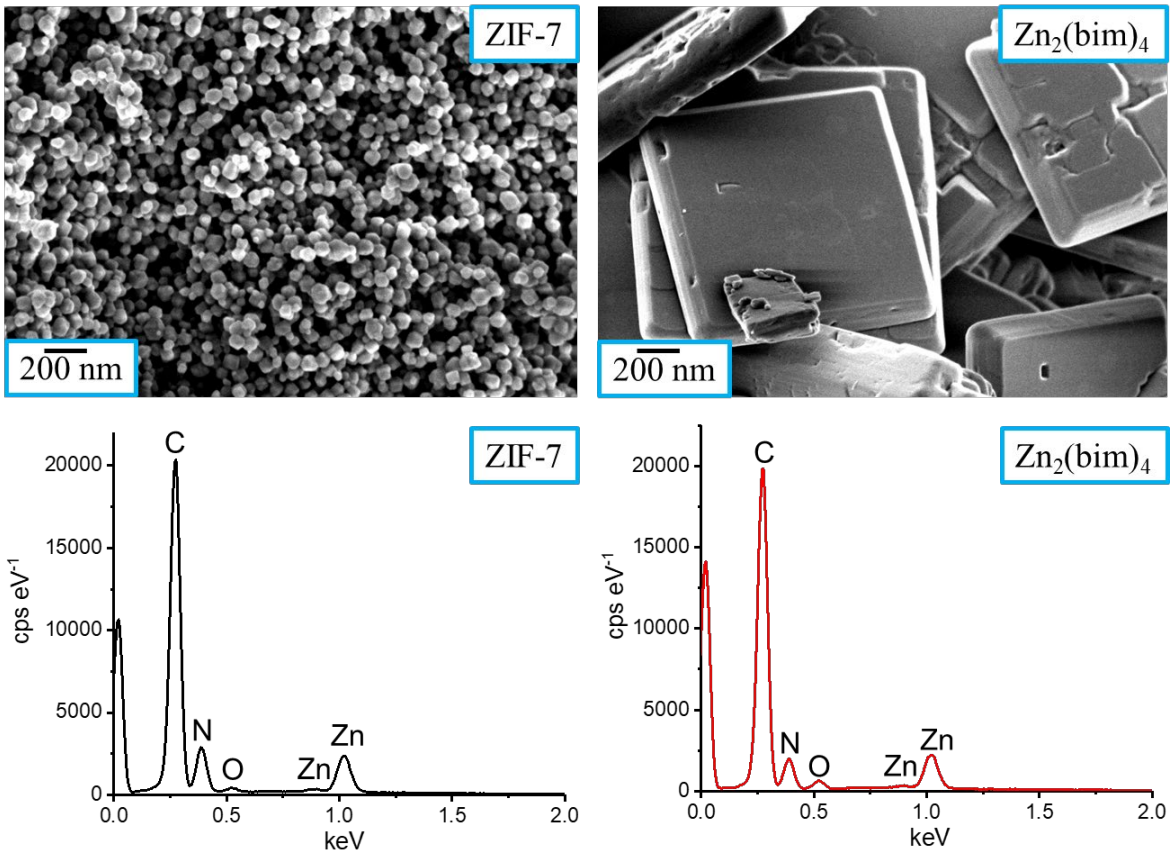

Figure 3. SEM images and EDX elemental mapping of the synthesized ZIF-7 and $Zn_2(bim)_4$ MOF particles.

The BET areas for ZIF-7, $Zn_2(bim)_4$, Mg-MOF-74, and MIL-53 samples are reported previously [15, 29, 40-41]. The BET area for TIFSIX-3 (Figure 4) was measured as 58 $m^2 g^{-1}$ that is lower than the literature data published for SIFSIX (223 $m^2 g^{-1}$), which is analogous of TIFSIX [36,

[42]. It seems that the porosity of the sample is low. The same behavior was seen in the case of SIFSIX-3-Ni [43].

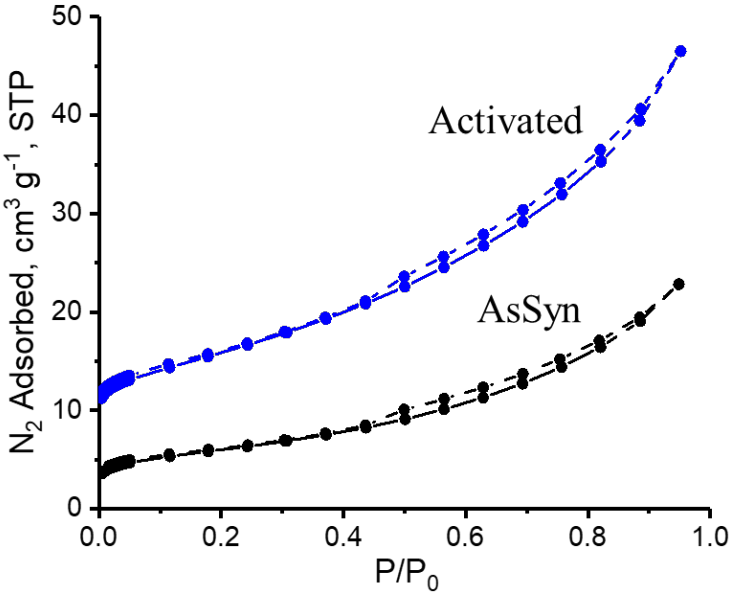

Figure 4. N_2-isotherms of TIFSIX-3 prepared in DMF at 85 °C AsSyn (black), after activation by (blue) Adsorption: solid line; Desorption: dashed line.

Morphology studies of the TFCMs. The cross-sectional structures of the thin-film composite membranes are shown in Figure 5. The Mg-MOF-74, MIL-53, and TIFSIX-3 particles are in micron range that require to control the crystal growth to reduce the size of the crystals to few nanometers. This will ensure controlling the incorporation of the filler into the polymer matrix and the formation of the defect-free selective layer of a TFC membrane. However, due to the presence of large particles inside the thin-film mixed-matrix membranes, defect zones are introduced between the polymer matrix and the particles, which lead to losses in gas transport performances of the proposed membranes. Therefore, the $Zn_2(bim)_4$ particles possess a layered structure that can undergo some degree of exfoliation during selective layer deposition, and the exfoliated layers could be oriented along the membrane surface. This phenomenon is expected due to the presence of shear force applied to the forming selective layer during TFC membrane

preparation. The capillary force applied by the porous support results in a strong suction of the solvent accompanying a complete wetting of the porous PAN sublayer, which gives an additional force for the orientation of the particles parallel to the membrane surface. Such forces were incapable for the penetration of the polymer into the porous PAN support due to the high molecular weight of PIM-1. A well-defined border line between the continuous polymer layer and porous substrate in the SEM images of the membranes (pure PIM-1 and MOF reinforced PIM-1 mixed-matrix membranes) supports our thesis. In order to see the dispersion of MOF particles in the polymer matrix, the cross-sectional EDX analysis were conducted and all data is presented in Figure S4. The metal centers were detected where the concentration of the metal atoms were measurable. During analysis, it was revealed that the concentration of Zn atoms was low and for this reason, the exfoliated $Zn_2(bim)_4$ nanosheets were undetectable.

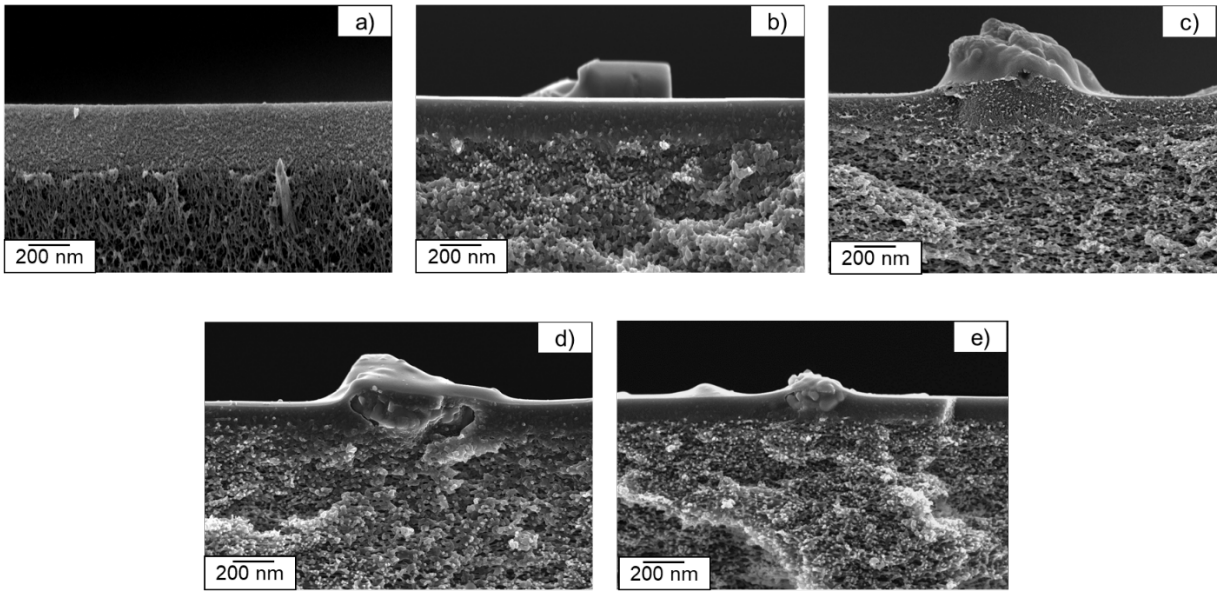

Figure 5. Cross-sectional SEM images of pure PIM-1 (a), PIM1-$Zn_2(bim)_4$_2 (b), PIM1-MOF74_8 (c), PIM1-MIL53_4 (d) and PIM1-TIFSIX3_4 (e) mixed-matrix membranes.

Gas separation results of the PIM-1/MOF thin-film composite mixed matrix membranes. Prepared TFC membranes whose selective layer consists of MOF incorporated PIM-1 as were used for the single gas transport experiments with H_2, CH_4, N_2, O_2, and CO_2 using in-house built gas permeation facility. Data of the single gas transport properties and the ideal selectivities of the prepared MMMs were obtained for at least four different stamps of the same membrane batch, and the permeances and selectivities were calculated as an average value of the 20 experimental points using the equations S2 and S3. The standard deviations and the mean values of the permeance were calculated on the base of the experimental results of four samples, and the ideal gas selectivity error was taken as a multiplication of the corresponding gas permeances. The experimental errors were determined based on the accuracy of the measurement system, which originates from the accuracy of permeate volume calibration, pressure and temperature sensors accuracy, determination of membrane surface. Permeability coefficients were derived from membrane permeance using selective layer thickness determined from the SEM cross-sectional images of membranes. Inputs for the selectivities and permeability coefficients and the comparison to the results with other PIM-1 and filler incorporated PIM-1 membranes are presented in Table 1 and Table S1. The membranes those showed better performances during the experiments are detailed in these tables. The results for 10 wt.% loading of Mg-MOF-74 and $Zn_2(bim)_4$ particles are shown as data for the aging experiments even though they showed low selectivities during experiments. However, this amount of loading was chosen for the aging experiments due to their comparable high permeabilities.

Table 1. Ideal selectivities for the MOF-incorporated PIM-1 TFC membranes. Experiments were conducted at 30 °C.

Membrane code	Filler	Wt.% of filler	Selectivities					Ref.
			H_2/N_2	CH_4/N_2	CO_2/N_2	O_2/N_2	CO_2/CH_4	
Literature data								
PIM-1	-	-	14.0	1.36	25.0	4.00	18.4	[44]
PIM-1/UiO-66	UiO-66	9	12.0	1.45	23.0	3.95	16.0	[24]
PIM-1/CAU-21-ODB	CAU-21-ODB	15	39.0	-	-	-	-	[45]
PIM-1/ZIF-67	ZIF-67	20	16.0	1.44	23.7	-	16.5	[46]
Experimental data of current study[‡]								
PIM-1	-	-	10.5	1.59	21.0	3.23	13.2	This work
PIM1-$Zn_2(bim)_4$_2	$Zn_2(bim)_4$	2	15.5	1.43	19.6	4.25	13.7	
PIM1-$Zn_2(bim)_4$_10	$Zn_2(bim)_4$	10	10.5	1.50	15.4	3.37	10.2	
PIM1-MOF74_8	Mg-MOF-74	8	16.1	1.40	17.1	4.12	12.2	
PIM1-MOF74_10	Mg-MOF-74	10	15.0	1.39	16.4	3.94	11.8	
PIM1-MIL53_4	MIL-53	4	18.3	1.34	17.0	4.00	12.7	
PIM1-TIFSIX3_4	TIFSIX-3	4	19.4	1.37	19.2	4.30	14.1	

[‡] 10 wt.% of loadings of Mg-MOF-74 and $Zn_2(bim)_4$ particles are shown here as data for aging experiments.

Tables and Figure S6 show that with the increase of the MOF particles loadings into the PIM-1 matrix, mainly, the selectivity of hydrogen over nitrogen increases. However, there is also a slight but statistically relevant increase in the selectivity of O_2/N_2 and almost non-changing selectivity for CO_2/N_2 and CH_4/N_2. The incorporation of the MOF particles into the PIM-1 matrix boosts the permeability of the mixed-matrix membranes (Table S1) for the gases investigated, except nitrogen in the cases of PIM1-Zn_2(bim)$_4$_2, PIM1-MIL53_4, and PIM1-TIFSIX3_4. We conducted the high-pressure adsorption experiments on the Mg-MOF-74 to understand the interaction of the particles with the gas molecules (Figure 6 and Figure S5).

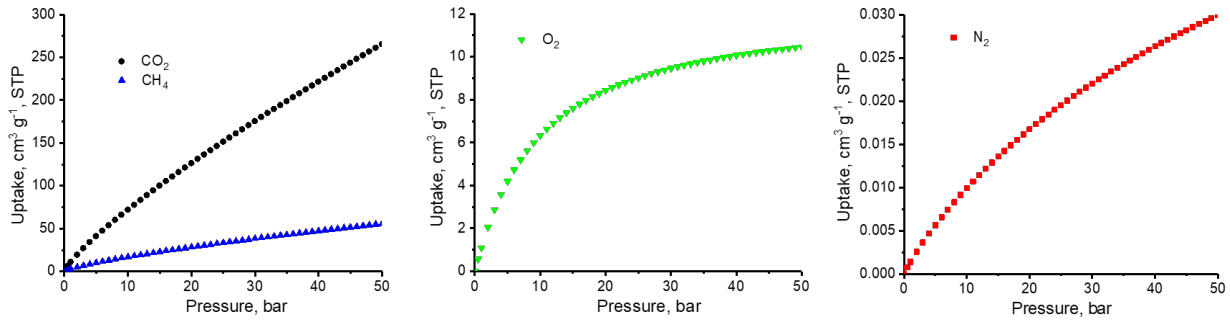

Figure 6. The Langmuir model adsorption isotherms of CO_2, CH_4, O_2, and N_2 for pristine Mg-MOF-74 based upon the experimental results (see Figure S5).

Table 2. The sorption model parameters of Mg-MOF-74 with comparison to the pristine PIM-1 taken from [47]. The C_H' and b parameters shown for Mg-MOF-74 was obtained by nonlinear least-squares fitting from Eq. S1.

Sample	Sorption model parameters	Feed gases			
		N_2	CH_4	O_2	CO_2
PIM-1[‡]	C_H', cm^3 (STP) cm^{-3}	-	62.1	-	104
	b, atm^{-1}	-	0.135	-	0.415
Mg-MOF-74	C_H', cm^3 (STP) g^{-1}	0.0758	12800	12.3	85600

	b, bar^{-1}	0.0185	0.0003	0.0972	0.0001

‡ The sorption model parameters for the pristine PIM-1 was calculated based upon a dual-mode sorption isotherm.

The experiment showed that Mg-MOF-74 has a strong affinity towards CO_2, while the adsorption of CH_4 is moderate. The adsorption of nitrogen and oxygen is much lower than the adsorption of carbon dioxide and methane. All the adsorption isotherms are well described by the nonlinear form of Langmuir equation [48].

This phenomenon can explain the reason for the high permeability coefficient for CO_2 in the PIM1-MOF74 MMM. We suggest that the permeance of CO_2 increases with the improved solubility of the gas in the composite membrane. Although there is no interaction of the particles with nitrogen, the permeance increases 1.4 times, which we claim that this is the effect of the 1.1 nm diameter nanochannels of Mg-MOF-74 particles. Considering this result, we suppose the other particles ($Zn_2(bim)_4$, MIL-53, and TIFSIX-3) trap the gas molecules inside the composite membrane, and the withdrawal of the gas becomes complicated. (Table 2).

At 2 wt.% loading of $Zn_2(bim)_4$, the increase in the permeability coefficients is seen in the cases of H_2, and O_2, while CO_2, N_2, and CH_4 permeabilities decrease (Figure S6). This gives an increase in the selectivities of hydrogen and oxygen over nitrogen. The selectivity of CO_2/N_2 is almost unchanged. This result is higher rather than the reported data in Table 1. Peng *et al.* [15] showed that $Zn_2(bim)_4$ particles are the stacked two-dimensional materials, and the layers have a ~0.21 nm pore diameter, which makes such kind materials as the potential candidates for hydrogen separation. The pore size effect could be supportive for the explanation of the selectivity increase in the mixed-matrix membranes of PIM1-MIL53_4 and PIM1-TIFSIX3_4, where the pore sizes of the particles are 0.7 and 0.4 nm, respectively. When these particles are incorporated into the

PIM-1 matrix, it is supposed to get mixed-matrix membranes prone to hydrogen separation. The H_2/CH_4 selectivity increased from ~6.6 for pure PIM-1 to ~11.0 for PIM1- $Zn_2(bim)_4$_2, to ~11.6 for PIM1-MOF74, to 13.7 for PIM1-MIL53_4 and to ~14.2 for PIM1-TIFSIX3_4 mixed-matrix membranes.

Table 3. The effect of MOF particles on the H_2/CO_2 selectivity with regard to penetrant size.

Gas molecule	Kinetic diameters, nm	H_2/CO_2 selectivities				
		PIM-1	PIM1- $Zn_2(bim)_4$_2	PIM1- MOF74_8	PIM1- MIL53_4	PIM1- TIFSIX3_4
H_2	0.289	0.52	0.79	0.94	1.1	1.0
CO_2	0.33					

Although hydrogen possesses small kinetic diameter (~0.289 nm), the permeability of pure PIM-1 follows the order of CO_2 (~0.33 nm) > H_2 (~0.289 nm) > O_2 (~0.346 nm) > CH_4 (~0.34 nm) > N_2 (~0.364 nm). It is worth noting that the reinforcement influences strongly on the gas transport properties of the mixed-matrix membrane (Figure S7). With the loading of MOF particles, the transport of hydrogen increases without any hindrance, while the transport of CO_2 decreases significantly. The reinforcement of PIM-1 with Mg-MOF-74 boosts the gas transport properties of the mixed-matrix membrane with a slight change in trend, which we claim that this is the result of either 1D nanochannels of Mg-MOF-74 or the defects formed between the polymer matrix and the nanoparticle. Table 3 shows how the particle loading affects H_2/CO_2 selectivities. The selectivity data is not relevant for the industrial applications; however, it shows a definite effect on the transport of these particular gas molecules. The CO_2 solubility of PIM-1 does not allow us to reach high separation factors for H_2/CO_2.

Figure S6 shows the effect of particle loadings on gas permeability coefficients of different mixed-matrix membranes, while Figure 7 shows the effect on the relative selectivities. As it is seen, with the increase of filler content in the membrane, the permeability coefficients increase, which is related to the introduction of the defect sites into the polymer matrix.

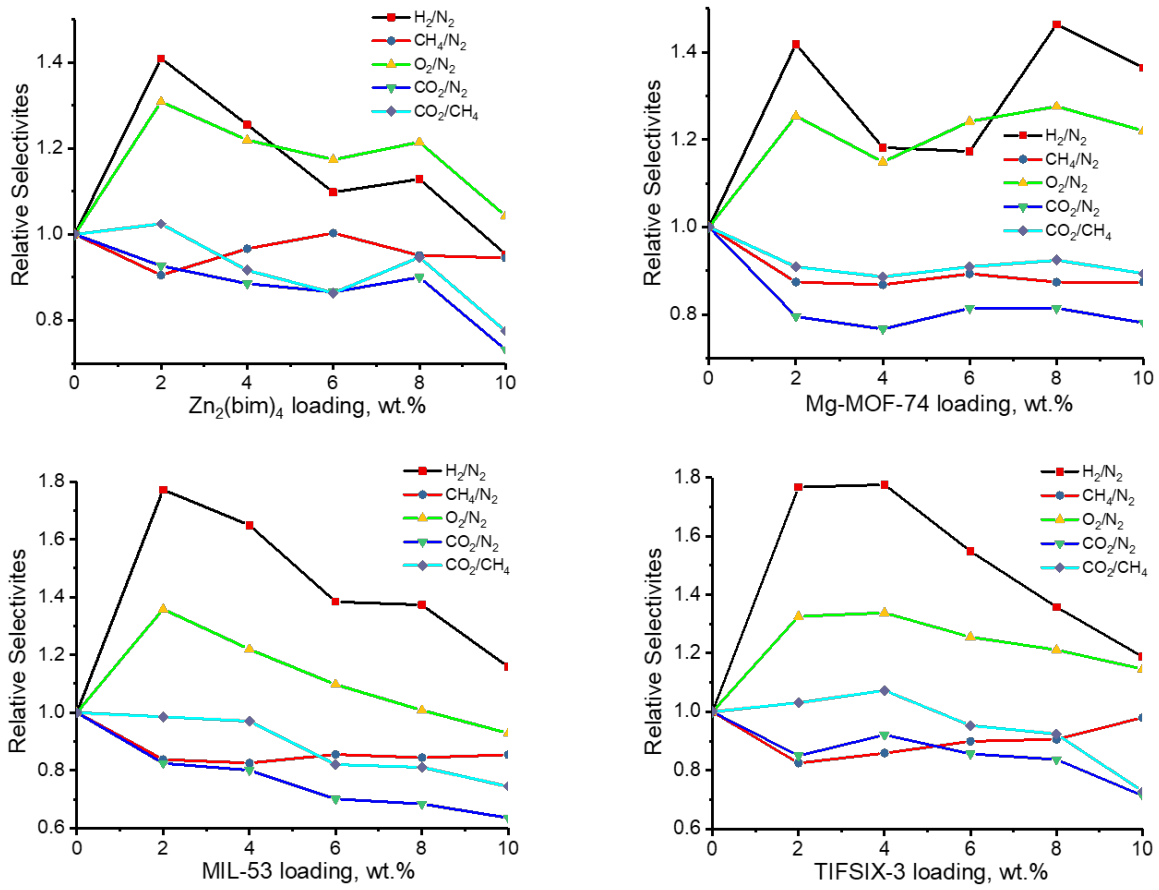

Figure 7. Relative selectivity of different gases as a function of MOF loadings in the PIM-1 polymer matrix.

In comparison to hydrogen, at 2 wt.% loading of $Zn_2(bim)_4$ particles, the transport of other gases is prohibited, which gives an increase in the corresponding selectivities. This can be explained by the exfoliation of some layered particles, which allows the transport of hydrogen. With the increase of the particle loading, the stacking effect of the layers allows other gases to by-

pass the nanoparticles giving rise in the permeabilities and decrease in the selectivities. The permeabilities of all gases stabilize between 6 wt.% and 8 wt.% that we claim after 8 wt.% loading the defect formation between the particles occurs and the gas molecules transport through such type of the defects. The same trend is observed in other fillers with a slight difference, which attributes to the nature of the particles. This could be explained by the introduction of defects zones inside the mixed-matrix membranes, which facilitate mass transport. This phenomenon is supported by the investigations of the relative selectivities as a function of MOF loading in PIM-1 (Figure 7).

Figure S8 shows that after incorporation of MOF particles into the PIM-1 polymer matrix, the mixed-matrix membranes transcend the 2008 Robeson upper bound except $Zn_2(bim)_4$ incorporated membrane.

Although the prepared membranes show promising properties, PIM-1 suffers from "physical aging" [49]. To understand the effect of the particle loadings on the aging of PIM-1, pure PIM-1, PIM1-MOF74_10, and PIM1-$Zn_2(bim)_4$_10 membranes were tested through nitrogen permeances. The membranes put for testing were cut 30 minutes after the membrane preparation as the start point. All the particle loadings were 10 wt.% with respect to polymer dry weight. The choice of the 10 wt.% loaded samples was related to their relatively high permeability coefficients than other counterparts even though their selectivities were low (Table 1). The cross-sectional SEM images of the MMMs used in aging experiments are shown in Figure S9.

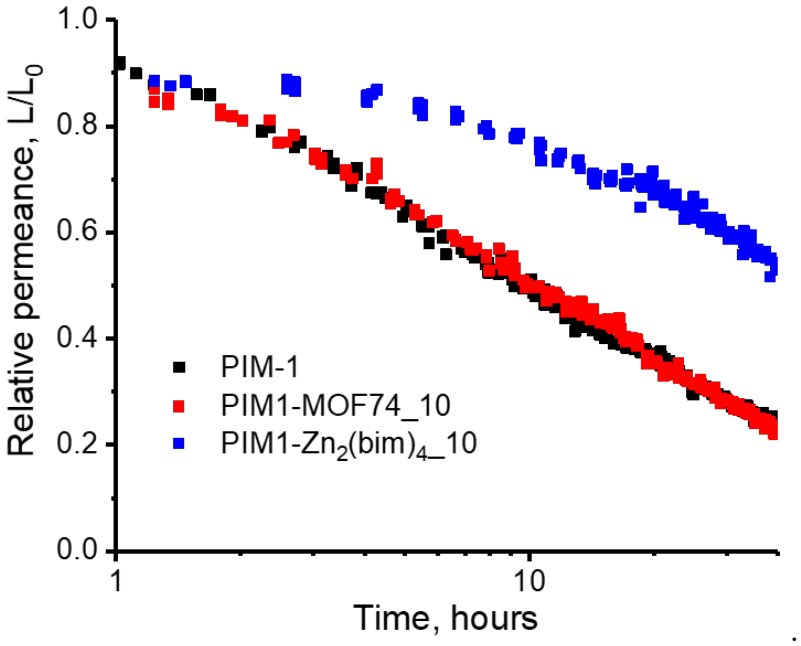

Figure 8. The aging behavior of pure PIM-1 and MOF-incorporated PIM-1 mixed-matrix membranes.

As it is evident from Figure 8, TFCM of PIM-1 ages drastically losing 50% of permeance in the first 10 hours of the experiment. When 10 wt.% of Mg-MOF-74 particles were incorporated into the PIM-1 polymer matrix, the aging trend followed the same path as pure PIM-1 TFCM. Interestingly, the $Zn_2(bim)_4$ 10 wt.% loading caused a very different effect on TFC membrane aging compared to the two aforementioned examples. The physical aging of PIM1-$Zn_2(bim)_4$_10 mixed-matrix membrane is ~40% less than pure PIM-1 and PIM1-MOF74_10 MMMs. This phenomenon could be explained by the exfoliation of the layered particles in the selective PIM-1 layer and formation of an enormous amount of polymer/particle interface which, probably has aging properties very different from bulk PIM-1. The later claim will further be analyzed after thorough exfoliation of the nanosheets.

CONCLUSIONS

Several metal-organic frameworks possessing two-dimensional and three-dimensional structures were synthesized and successfully characterized by SSNMR, FTIR, XRD, BET, etc. XRD analysis showed that all synthesized MOFs have a high crystallinity degree. The high-pressure adsorption experiments conducted on Mg-MOF-74 showed that such kind of particles adsorbs CO_2 much higher than other gases. Gas separation experiments revealed that when MOF particles incorporate into the PIM-1 matrix, the gas separation performances of the latest boosts and the obtained mixed-matrix membranes transcend the 2008 Robeson upper bound. Such membranes can be good candidates for ammonia purge gas, oxygen enrichment, and acid gas treatment applications. Layered MOF crystals showed improved performances against the aging of PIM-1, and the experiments in this will be continued in the future.

The results could answer the questions arisen in the introduction part of the manuscript. Thus:

a) Two-dimensional layered materials can be exfoliated in the polymer matrix rather than three-dimensional particles, which gives us to use the low amount of the compound for better gas transport properties.
b) It was revealed that the incorporation of the microporous particles into the PIM-1 polymer matrix considerably influences the permeability coefficients and selectivities of hydrogen and oxygen over nitrogen. Such result improves the gas transport properties of PIM-1.
c) Having 0.2 nm pore diameter, the layered $Zn_2(bim)_4$ is exfoliated in the polymer matrix and this factor influences the aging of the membrane, which might be useful for the sustainability character of the industrial progress.

ASSOCIATED CONTENT

Supporting Information

The following files are available free of charge on the ACS Publications website at DOI: .

Characterization methods, Permeability coefficients for the MOF containing PIM-1 TFC membranes, TEM images of layered $Zn_2(bim)_4$ and single-layer $Zn_2(bim)_4$ nanosheet after exfoliation, Cross-sectional EDX elemental mapping for the prepared thin-film composite membranes, The experimental adsorption isotherms of CO_2, CH_4, O_2, and N_2 in pristine Mg-MOF-74, Gas permeability coefficients of different gases as a function of MOF content in PIM-1, and The SEM images of the MMMs of PIM-1 and Mg-MOF-74 (left), and PIM-1 and $Zn_2(bim)_4$ (right) particles used in long-term aging experiments brief description (PDF).

Author Contributions

The manuscript was written through contributions of all authors. All authors have given approval to the final version of the manuscript. [†]**Elvin Aliyev:** Synthesis of ZIF-7 and $Zn_2(bim)_4$ particles and their analysis, Data curation, Membrane preparation, Conceptualization, Gas separation experiments, Writing-original draft. [‡]**Jan Warfsmann:** Synthesis of Mg-MOF-74, MIL-53, and TIFSIX-3 particles and their analysis. [‡]**Begum Tokay:** Writing-review and editing. [†]**Sergey Shishatskiy:** Scientific discussion, Writing-review and editing. [§]**Young Joo Lee:** Solid-state nuclear magnetic resonance experiments and the discussion of the results, Writing-review and editing. [†]**Jelena Lillepaerg:** Adsorption experiments, Writing-review and editing. [‡]**Neil R. Champness:** Writing-review and editing. [†]**Volkan Filiz:** Scientific discussion, Writing-review and editing.

Funding Sources

There is no any funding for this work to be declared.

Notes

The authors declare no competing interests.

ACKNOWLEDGMENT

BT, NRC and JW thank the University of Nottingham the Nanoscale and Microscale Centre (nmRC) for providing access to instrumentation. The authors appreciate the valuable comments of Prof. Volker Abetz and thank him for scientific discussions. We cordially thank Clarissa Abetz for her help in conduction the SEM experiments and their interpretations. The authors also thank Anke-Lisa Hoehme and Erik Schneider for their valuable efforts in the SEM investigations.

ABBREVIATIONS

PIM, polymer of intrinsic microporosity; MOF, metal-organic framework; TFCM, thin-film composite membrane; FTIR, fourier-transform infrared spectroscopy; SSNMR, solid-state NMR; XRD, X-ray diffraction; TGA, thermogravimetric analysis; SEM, scanning electron microscopy; MMM, mixed matrix membrane; H_4DHTP, 2,5-dihydroxyterephthalic acid; DMF, *N,N*-Dimethylformamide; MeOH, methanol; DI water, deionized water; RT, room temperature; PAN, polyacrylonitrile; ATR, attenuated total reflectance; CP, cross-polarization; MAS, magic-angle spinning; XRD, X-ray diffraction; MSB, magnetic suspension balance.

REFERENCES

1. Robeson, L. M., The upper bound revisited. *Journal of Membrane Science* **2008,** *320* (1), 390-400, DOI: 10.1016/j.memsci.2008.04.030

2. Santi Kulprathipanja, R. W. N., Norman N. Li Separation of fluids by means of mixed matrix membranes. 1988.

3. KULPRATHIPANJA, S., Mixed Matrix Membrane Development. *Annals of the New York Academy of Sciences* **2003,** *984* (1), 361-369, DOI: 10.1111/j.1749-6632.2003.tb06012.x.

4. Prasad, B.; Mandal, B., Graphene-Incorporated Biopolymeric Mixed-Matrix Membrane for Enhanced CO2 Separation by Regulating the Support Pore Filling. *ACS Applied Materials & Interfaces* **2018,** *10* (33), 27810-27820, DOI: 10.1021/acsami.8b09377.

5. Aliyev, E. M.; Khan, M. M.; Nabiyev, A. M.; Alosmanov, R. M.; Bunyad-zadeh, I. A.; Shishatskiy, S.; Filiz, V., Covalently Modified Graphene Oxide and Polymer of Intrinsic Microporosity (PIM-1) in Mixed Matrix Thin-Film Composite Membranes. *Nanoscale Research Letters* **2018,** *13* (1), 359, DOI: 10.1186/s11671-018-2771-3.

6. Ma, W.; Chen, T.; Nanni, S.; Yang, L.; Ye, Z.; Rahaman, M. S., Zwitterion-Functionalized Graphene Oxide Incorporated Polyamide Membranes with Improved Antifouling Properties. *Langmuir* **2019,** *35* (5), 1513-1525, DOI: 10.1021/acs.langmuir.8b02044.

7. Wang, X.; Zhao, Y.; Tian, E.; Li, J.; Ren, Y., Graphene Oxide-Based Polymeric Membranes for Water Treatment. *Advanced Materials Interfaces* **2018,** *5* (15), 1701427, DOI: 10.1002/admi.201701427.

8. Budd, P. M.; McKeown, N. B.; Ghanem, B. S.; Msayib, K. J.; Fritsch, D.; Starannikova, L.; Belov, N.; Sanfirova, O.; Yampolskii, Y.; Shantarovich, V., Gas permeation parameters and other physicochemical properties of a polymer of intrinsic microporosity: Polybenzodioxane PIM-1. *Journal of Membrane Science* **2008,** *325* (2), 851-860, DOI: 10.1016/j.memsci.2008.09.010.

9. Rahman, M. M.; Filiz, V.; Khan, M. M.; Gacal, B. N.; Abetz, V., Functionalization of POSS nanoparticles and fabrication of block copolymer nanocomposite membranes for CO2 separation. *Reactive and Functional Polymers* **2015,** *86*, 125-133, DOI: 10.1016/j.reactfunctpolym.2014.07.006.

10. Khan, M. M.; Filiz, V.; Bengtson, G.; Shishatskiy, S.; Rahman, M.; Abetz, V., Functionalized carbon nanotubes mixed matrix membranes of polymers of intrinsic microporosity for gas separation. *Nanoscale Research Letters* **2012,** *7* (1), 504, DOI: 10.1186/1556-276X-7-504.

11. Llewellyn, P.; Maurin, G.; Rouquerol, J., 14 - Adsorption by Metal-Organic Frameworks. In *Adsorption by Powders and Porous Solids (Second Edition)*, Rouquerol, F.; Rouquerol, J.; Sing, K. S. W.; Llewellyn, P.; Maurin, G., Eds. Academic Press: Oxford, 2014; pp 565-610.

12. Akpinar, I.; Yazaydin, A. O., Adsorption of Atrazine from Water in Metal–Organic Framework Materials. *Journal of Chemical & Engineering Data* **2018,** *63* (7), 2368-2375, DOI: 10.1021/acs.jced.7b00930.

13. Xie, K.; Fu, Q.; Xu, C.; Lu, H.; Zhao, Q.; Curtain, R.; Gu, D.; Webley, P. A.; Qiao, G. G., Continuous assembly of a polymer on a metal–organic framework (CAP on MOF): a 30 nm thick polymeric gas separation membrane. *Energy & Environmental Science* **2018,** *11* (3), 544-550, DOI: 10.1039/C7EE02820B.

14. Jang, E.; Kim, E.; Kim, H.; Lee, T.; Yeom, H.-J.; Kim, Y.-W.; Choi, J., Formation of ZIF-8 membranes inside porous supports for improving both their H2/CO2 separation performance and thermal/mechanical stability. *Journal of Membrane Science* **2017,** *540*, 430-439, DOI: 10.1016/j.memsci.2017.06.072.

15. Peng, Y.; Li, Y.; Ban, Y.; Jin, H.; Jiao, W.; Liu, X.; Yang, W., Metal-organic framework nanosheets as building blocks for molecular sieving membranes. *Science* **2014,** *346* (6215), 1356-1359, DOI: 10.1126/science.1254227.

16. Li, H.; Li, L.; Lin, R.-B.; Ramirez, G.; Zhou, W.; Krishna, R.; Zhang, Z.; Xiang, S.; Chen, B., Microporous Metal–Organic Framework with Dual Functionalities for Efficient Separation of Acetylene from Light Hydrocarbon Mixtures. *ACS Sustainable Chemistry & Engineering* **2019,** *7* (5), 4897-4902, DOI: 10.1021/acssuschemeng.8b05480.

17. Go, Y.; Lee, J. H.; Shamsudin, I. K.; Kim, J.; Othman, M. R., Microporous ZIF-7 membranes prepared by in-situ growth method for hydrogen separation. *International Journal of Hydrogen Energy* **2016,** *41* (24), 10366-10373, DOI: 10.1016/j.ijhydene.2015.09.060.

18. Adatoz, E.; Avci, A. K.; Keskin, S., Opportunities and challenges of MOF-based membranes in gas separations. *Separation and Purification Technology* **2015,** *152*, 207-237, DOI: 10.1016/j.seppur.2015.08.020.

19. Tien-Binh, N.; Vinh-Thang, H.; Chen, X. Y.; Rodrigue, D.; Kaliaguine, S., Crosslinked MOF-polymer to enhance gas separation of mixed matrix membranes. *Journal of Membrane Science* **2016,** *520*, 941-950, DOI: 10.1016/j.memsci.2016.08.045.

20. Yu, S.; Li, S.; Huang, S.; Zeng, Z.; Cui, S.; Liu, Y., Covalently bonded zeolitic imidazolate frameworks and polymers with enhanced compatibility in thin-film nanocomposite membranes for gas separation. *Journal of Membrane Science* **2017,** *540*, 155-164, DOI: 10.1016/j.memsci.2017.06.047.

21. Safak Boroglu, M.; Yumru, A. B., Gas separation performance of 6FDA-DAM-ZIF-11 mixed-matrix membranes for H2/CH4 and CO2/CH4 separation. *Separation and Purification Technology* **2017,** *173*, 269-279, DOI: 10.1016/j.seppur.2016.09.037.

22. Japip, S.; Wang, H.; Xiao, Y.; Shung Chung, T., Highly permeable zeolitic imidazolate framework (ZIF)-71 nano-particles enhanced polyimide membranes for gas separation. *Journal of Membrane Science* **2014,** *467*, 162-174, DOI: 10.1016/j.memsci.2014.05.025.

23. Cheng, Y.; Wang, X.; Jia, C.; Wang, Y.; Zhai, L.; Wang, Q.; Zhao, D., Ultrathin mixed matrix membranes containing two-dimensional metal-organic framework nanosheets for efficient CO2/CH4 separation. *Journal of Membrane Science* **2017,** *539*, 213-223, DOI: 10.1016/j.memsci.2017.06.011.

24. Khdhayyer, M. R.; Esposito, E.; Fuoco, A.; Monteleone, M.; Giorno, L.; Jansen, J. C.; Attfield, M. P.; Budd, P. M., Mixed matrix membranes based on UiO-66 MOFs in the polymer of intrinsic microporosity PIM-1. *Separation and Purification Technology* **2017,** *173*, 304-313, DOI: 10.1016/j.seppur.2016.09.036.

25. Wang, Z.; Wang, D.; Zhang, S.; Hu, L.; Jin, J., Interfacial Design of Mixed Matrix Membranes for Improved Gas Separation Performance. *Advanced Materials* **2016,** *28* (17), 3399-3405, DOI: 10.1002/adma.201504982.

26. Li, C.; Wu, C.; Zhang, B., Enhanced CO2/CH4 Separation Performances of Mixed Matrix Membranes Incorporated with Two-Dimensional Ni-Based MOF Nanosheets. *ACS Sustainable Chemistry & Engineering* **2020,** *8* (1), 642-648, DOI: 10.1021/acssuschemeng.9b06370.

27. Etxeberria-Benavides, M.; David, O.; Johnson, T.; Łozińska, M. M.; Orsi, A.; Wright, P. A.; Mastel, S.; Hillenbrand, R.; Kapteijn, F.; Gascon, J., High performance mixed matrix membranes (MMMs) composed of ZIF-94 filler and 6FDA-DAM polymer. *Journal of Membrane Science* **2018,** *550*, 198-207, DOI: 10.1016/j.memsci.2017.12.033.

28. Campbell, J.; Tokay, B., Controlling the size and shape of Mg-MOF-74 crystals to optimise film synthesis on alumina substrates. *Microporous and Mesoporous Materials* **2017,** *251*, 190-199, DOI: 10.1016/j.micromeso.2017.05.058.

29. Warfsmann, J.; Tokay, B.; Champness, N. R., Synthesis of hydrophobic MIL-53(Al) nanoparticles in low molecular weight alcohols: systematic investigation of solvent effects. *CrystEngComm* **2018,** *20* (32), 4666-4675, DOI: 10.1039/C8CE00913A.

30. J. Warfsman, B. T., N. R. Champness, Thin-film synthesis of hybrid ultramicroporous materials (HUMs)- A comparative approach. *Microporous and Mesoporous Materials **2020**, 311,* 110686, DOI: 10.1016/j.micromeso.2020.110686.

31. Grunauer, J.; Filiz, V.; Shishatskiy, S.; Abetz, C.; Abetz, V., Scalable application of thin-film coating techniques for supported liquid membranes for gas separation made from ionic liquids. *Journal of Membrane Science* **2016,** *518*, 178-191, DOI: 10.1016/j.memsci.2016.07.005.

32. Pashchevskaya, N. V.; Nazarenko, M. A.; Bolotin, S. N.; Oflidi, A. I.; Panyushkin, V. T., Effect of the condition of synthesis on the composition and structure of copper(II) complexes with benzimidazole. *Russian Journal of Inorganic Chemistry* **2010,** *55* (9), 1425-1432, DOI: 10.1134/S0036023610090159.

33. Mohan, S.; Sundaraganesan, N.; Mink, J., FTIR and Raman studies on benzimidazole. *Spectrochimica Acta Part A: Molecular Spectroscopy* **1991,** *47* (8), 1111-1115, DOI: 10.1016/0584-8539(91)80042-H.

34. Sneddon, S.; Kahr, J.; Orsi, A. F.; Price, D. J.; Dawson, D. M.; Wright, P. A.; Ashbrook, S. E., Investigation of zeolitic imidazolate frameworks using 13C and 15N solid-state NMR spectroscopy. *Solid State Nuclear Magnetic Resonance* **2017,** *87*, 54-64, DOI: 10.1016/j.ssnmr.2017.09.001.

35. Du, Y.; Mao, K.; Wooler, B.; Sharma, A. K.; Colmyer, D.; Nines, M.; Weston, S. C., Insights into the Flexibility of ZIF-7 and Its Structural Impact in Alcohol Adsorption. *The Journal of Physical Chemistry C* **2017,** *121* (50), 28090-28095, DOI: 10.1021/acs.jpcc.7b10339.

36. Kumar, A.; Hua, C.; Madden, D. G.; O'Nolan, D.; Chen, K.-J.; Keane, L.-A. J.; Perry, J. J.; Zaworotko, M. J., Hybrid ultramicroporous materials (HUMs) with enhanced stability and trace carbon capture performance. *Chemical Communications* **2017,** *53* (44), 5946-5949, DOI: 10.1039/C7CC02289A.

37. Wu, X.; Bao, Z.; Yuan, B.; Wang, J.; Sun, Y.; Luo, H.; Deng, S., Microwave synthesis and characterization of MOF-74 (M=Ni, Mg) for gas separation. *Microporous and Mesoporous Materials* **2013,** *180*, 114-122, DOI: 10.1016/j.micromeso.2013.06.023.

38. Wang, N.; Mundstock, A.; Liu, Y.; Huang, A.; Caro, J., Amine-modified Mg-MOF-74/CPO-27-Mg membrane with enhanced H2/CO2 separation. *Chemical Engineering Science* **2015,** *124*, 27-36, DOI: 10.1016/j.ces.2014.10.037.

39. Loiseau, T.; Serre, C.; Huguenard, C.; Fink, G.; Taulelle, F.; Henry, M.; Bataille, T.; Férey, G., A Rationale for the Large Breathing of the Porous Aluminum Terephthalate (MIL-53) Upon Hydration. *Chemistry – A European Journal* **2004,** *10* (6), 1373-1382, DOI: 10.1002/chem.200305413.

40. Majumdar, S.; Tokay, B.; Martin-Gil, V.; Campbell, J.; Castro-Muñoz, R.; Ahmad, M. Z.; Fila, V., Mg-MOF-74/Polyvinyl acetate (PVAc) mixed matrix membranes for CO2 separation. *Separation and Purification Technology* **2020,** *238*, 116411, DOI: 10.1016/j.seppur.2019.116411.

41. Wu, X.; Niknam Shahrak, M.; Yuan, B.; Deng, S., Synthesis and characterization of zeolitic imidazolate framework ZIF-7 for CO2 and CH4 separation. *Microporous and Mesoporous Materials* **2014,** *190*, 189-196, DOI: 10.1016/j.micromeso.2014.02.016.

42. Chen, K.-J.; Scott, Hayley S.; Madden, David G.; Pham, T.; Kumar, A.; Bajpai, A.; Lusi, M.; Forrest, Katherine A.; Space, B.; Perry, John J.; Zaworotko, Michael J., Benchmark C2H2/CO2 and CO2/C2H2 Separation by Two Closely Related Hybrid Ultramicroporous Materials. *Chem* **2016,** *1* (5), 753-765, DOI: 10.1016/j.chempr.2016.10.009.

43. Elsaidi, S. K.; Venna, S. R.; Mohamed, M. H.; Gipple, M. J.; Hopkinson, D. P., Dual-Layer MOF Composite Membranes with Tuned Interface Interaction for Postcombustion Carbon Dioxide Separation. *Cell Reports Physical Science* **2020,** *1* (5), 100059, DOI: 10.1016/j.xcrp.2020.100059.

44. Budd, P. M.; Msayib, K. J.; Tattershall, C. E.; Ghanem, B. S.; Reynolds, K. J.; McKeown, N. B.; Fritsch, D., Gas separation membranes from polymers of intrinsic microporosity. *Journal of Membrane Science* **2005,** *251* (1), 263-269, DOI: 10.1016/j.memsci.2005.01.009.

45. Zhang, C.; Liu, B.; Wang, G.; Yu, G.; Zou, X.; Zhu, G., Small-pore CAU-21 and porous PIM-1 in mixed-matrix membranes for improving selectivity and permeability in hydrogen separation. *Chemical Communications* **2019,** *55* (49), 7101-7104, DOI: 10.1039/C9CC02537E.

46. Wu, X.; Liu, W.; Wu, H.; Zong, X.; Yang, L.; Wu, Y.; Ren, Y.; Shi, C.; Wang, S.; Jiang, Z., Nanoporous ZIF-67 embedded polymers of intrinsic microporosity membranes with enhanced gas separation performance. *Journal of Membrane Science* **2018,** *548*, 309-318, DOI: 10.1016/j.memsci.2017.11.038.

47. Khan, M. M.; Shishatskiy, S.; Filiz, V., Mixed Matrix Membranes of Boron Icosahedron and Polymers of Intrinsic Microporosity (PIM-1) for Gas Separation. *Membranes* **2018,** *8* (1), 1, DOI: 10.3390/membranes8010001.

48. Liu, L.; Luo, X.-B.; Ding, L.; Luo, S.-L., 4 - Application of Nanotechnology in the Removal of Heavy Metal From Water. In *Nanomaterials for the Removal of Pollutants and Resource Reutilization*, Luo, X.; Deng, F., Eds. Elsevier: 2019; pp 83-147.

49. Müller, N.; Handge, U. A.; Abetz, V., Physical ageing and lifetime prediction of polymer membranes for gas separation processes. *Journal of Membrane Science* **2016,** *516*, 33-46, DOI: 10.1016/j.memsci.2016.05.055.